Hyperspectral Imaging of Localized, Optically-Active Defects in GaAs Solar Cells

Behrang H. Hamadani[1], Margaret A. Stevens[2], Brianna Conrad[1], Matthew P. Lumb[3], Eric Armour[4], and Kenneth J. Schmieder[5]

[1]National Institute of Standards and Technology, Gaithersburg, MD 20899 USA
[2]NRC Postdoc Residing at NRL, Washington, DC 20375 USA
[3]Formerly with George Washington University, Washington, DC 20052 USA
[4]Veeco Instruments, Somerset, NJ 08873 USA
[5]U.S. Naval Research Laboratory, Washington, DC 20375 USA

Abstract—**A novel hyperspectral imaging instrument with dual electroluminescence and photoluminescence capability was used to image and analyze localized radiative defects in rear-junction GaAs solar cells grown at 1 µm/min. The absolute photon emission rates were measured over a wide spectral range encompassing both the sub-band gap region and the higher photon energies, resolving spatial features on the order of 1 µm with complete spectral information. We find that some radiative defects are pinholes in the GaAs active layer, transmitting luminescence signal from other buried device layers. More notably, we observe the formation of a high-intensity, halo-like defect band in the vicinity of some of these processing-related defects. Such defects show a characteristic double-peak emission with maxima at 870 nm and 894 nm at room temperature corresponding to the band-to-band and the band-to-impurity optical transitions respectively. These sub-band gap radiative regions are likely gallium antisite defects and are thought to form shallow impurity bands within the band gap.**

Keywords—hyperspectral imaging, defects, GaAs solar cells, radiative defects, photoluminescence.

I. INTRODUCTION

Hyperspectral (HS) imaging is a convenient wide-field technique that combines spectroscopy and imaging to obtain a spectrum for each pixel of an image [1], [2]. Given the appropriate spectral and spatial resolution, HS imaging in either electroluminescence (EL) or photoluminescence (PL) modes can be used to obtain the full spectral emission information of visualized local defects or regions of heterogeneity across the active layer of a solar cell [3]. Traditional mapping techniques such as micro-PL can provide high-resolution images under a scanning optical microscope; however, such techniques are time-consuming and injection levels are locally very high [4]. Given appropriate illumination and collection optics and camera pixel size and sensitivity, HS wide-field imaging can be performed at intensities well under 10 mW/cm^2, spatial resolution of < 1 µm, and a spectral resolution of ≈ 1 nm. If the HS imager is calibrated by use of radiometric standards to measure the absolute photon emission rates, i.e., photons/m^2·s·eV for each photon energy E, then the generalized Planck law can be used to calculate local Fermi level splitting energy, local radiative efficiency (if incident photon flux is known) and other important device-related parameters [5], [6].

Although luminescence-based imaging techniques will only reveal the location and the intensity of radiative transitions in semiconductor materials, such observations could also indicate nonradiative centers or local shunts across a device and will reveal how the voltage or current flow is affected around a particular local defect or region. In this paper, we report a novel radiative defect halo that is (mostly) formed at locations of processing-related defects within the active GaAs emitter layer of rear-junction solar cells. The high growth rate of the active layer makes these cells particularly susceptible to local defect formations. We believe these defects are gallium antisite or vacancy defects that are formed in large concentrations at the locations shown. These types of defects are usually more prominent at lower temperatures due to the temperature-activated nature of the transition; however, with high enough concentration, they can be spectrally resolved even at room temperature. The temperature evolution of one such defect will also be briefly discussed.

II. METHODS

A. Device fabrication and structure

The devices were grown using a K475i Veeco MOCVD tool [7]. The precursors were trimethylgallium (TMGa), trimethylindium (TMIn), trimethylaluminum (TMAl), arsine (AsH$_3$), phosphine (PH$_3$), disilane (Si$_2$H$_6$), diethyltellurium (DETe), carbon tetrabromide (CBr$_4$), and dimethylzinc (DMZn). GaAs emitter and base growth rate was approximately 1 µm/min. The GaAs V/III ratio was 9. Growth temperature varied between 640 °C to 680 °C, and chamber pressure was held at 42 Torr. GaAs substrates were (100) 5° offcut toward <011> p-type. Solar cells were grown above an AlGaAs distributed Bragg reflector (DBR) with a stop-band nominally centered at 850 nm. Devices were fabricated with standard lithographic and wet etch processes into mesas of 5 mm×5 mm. Device structure is shown in the inset of Fig. 2. Further structure details and process information can be found in reference [6].

B. Device measurements and characterization

The solar cells were wire-bonded and characterized using current vs voltage (*I-V*), external quantum efficiency (EQE), and external radiative efficiency (ERE) measurements. The typical
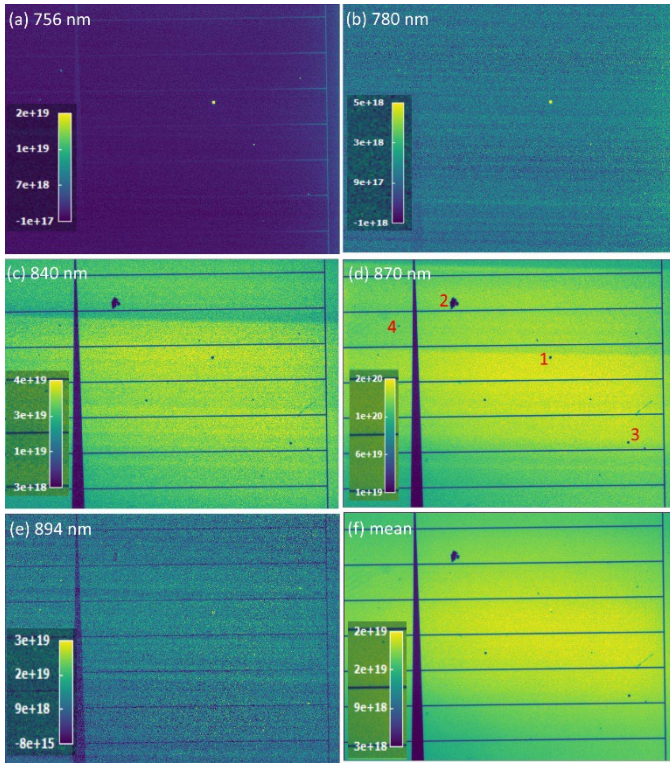
Fig. 1. Absolute PL images of a rear-junction GaAs solar cell at several wavelengths (a-e) and the mean PL image (f) obtained under the 5× objective. The FOV is ≈ 3.5 mm. Emission rates are in photons/(m²·s·eV).

open circuit voltage V_{oc} and the short circuit current I_{sc} under air mass 1.5 G illumination for these cells were 1.032 V and 26.8 mA/cm², respectively, with the power conversion efficiency (PCE) at ≈ 22.55 % but higher performance has been reported previously [8], [9]. The EQE at 840 nm is at 93.7 %, and the average device ERE at a laser illumination intensity of ≈ 700 W/m² is about 1 %, which is comparable with other GaAs devices of similar PCE that have been tested in our lab. Our expanded uncertainty in PCE measurements is about 1 % and the ERE measurements are accurate to about ± 15 %.

C. Hyperspectral characterization

HS imaging in both PL and EL modes was performed using a wide-field imaging system with capability to scan the spectral region of 400 nm-1600 nm using two camera systems. In this paper, only PL images are shown and discussed. The various objective lenses allow for a field of view (FOV) ranging from 160 mm to less than 500 μm. In the 400 nm to 1000 nm region, the spectral resolution is better than 2 nm. For PL excitation, a 532 nm laser is used to uniformly illuminate the entire FOV, with laser intensities depending on the objective, neutral density filter, and the laser power setting. The reported data here are all at laser intensities in the range of 100 mW/cm² to 800 mW/cm². The absolute calibration of the imager is discussed elsewhere [5]. Temperature dependent imaging was performed with a liquid nitrogen-flow optical cryostat under vacuum.

III. RESULTS

Figure 1(a-e) shows a series of absolute PL images, taken with a 5 × objective at several wavelengths, with the colorbar

showing the absolute photon emission rates. The dark horizontal gridlines and the thicker vertical line are the top electrode contact, with 350 μm spacing between the horizonal lines. Since the band-to-band (BB) transition in GaAs is at ≈ 870 nm (1.425 eV), no emission should be visible in the 756 nm (Fig. 1(a)) image. A closer examination however reveals several bright spots where a significant signal is recorded. These spots mostly fade out at 780 nm. The 840 nm and the 870 nm images show large bright areas across the device corresponding to the BB signal with emission rates strongest at 870 nm. The 756-nm bright spots are now mostly dark, indicating little BB signal at those sites. There are also additional defects appearing dark in these images.

Examination of Fig. 1(e) at 894 nm reveals a faint, doughnut-shaped signal at the location of some of the dark spots, particularly those present at 756 nm, which is discussed next. One final observation here is that the mean PL signal (averaged over all the wavelengths from 700 nm to 950 nm), as shown in Fig. 1(f) is not sufficient to show all the nuances that the hyperspectral imaging has revealed.

The complete emission spectra from inside the 4 localized defects as labelled in Fig. 1(d) and also the whole-cell PL signal are shown in Fig. 2. The most prominent of these defects is *defect 1*, which shows a substantial peak at 756 nm, much more intense than its peak at 870 nm, which is the reason why it appears very bright in Fig. 1(a) but dark in Fig. 1(d). Others such as *defect 4* also show the 756 nm peak, though at a smaller rate. We have concluded that these defects are pinhole defects that transmit the PL signal associated with the buried DBR layer up to the top, as verified by independent DBR-only PL measurements. It is likely that the pinholes originate from imperfections in the photoresist mask during the fabrication process, but they could also be related to defect formation during the fast growth conditions of these devices. Some other defects such as *defect 2* and *defect 3* show little to none of the 756 nm signal, and hence are not pinholes but likely areas of low-quality GaAs growth. The whole-cell signal does not seem to be affected much by the deep pinholes since there are only a few of
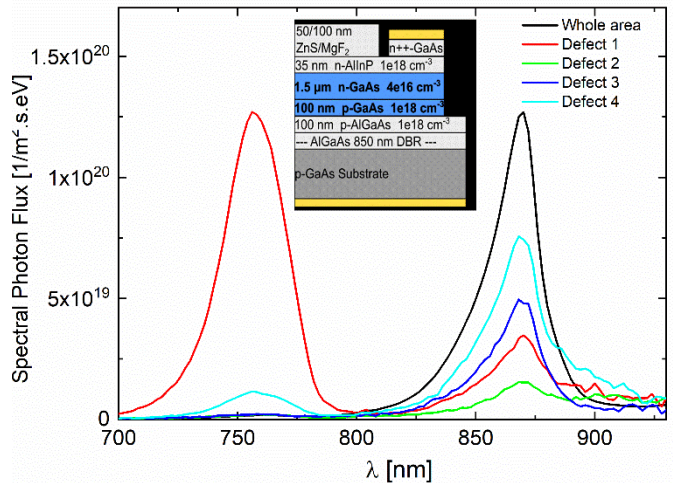

Fig. 2. (Inset) device structure. (main) The PL emission spectra from several defect sites labelled in Fig. 1(d) and also the whole-area PL signal.
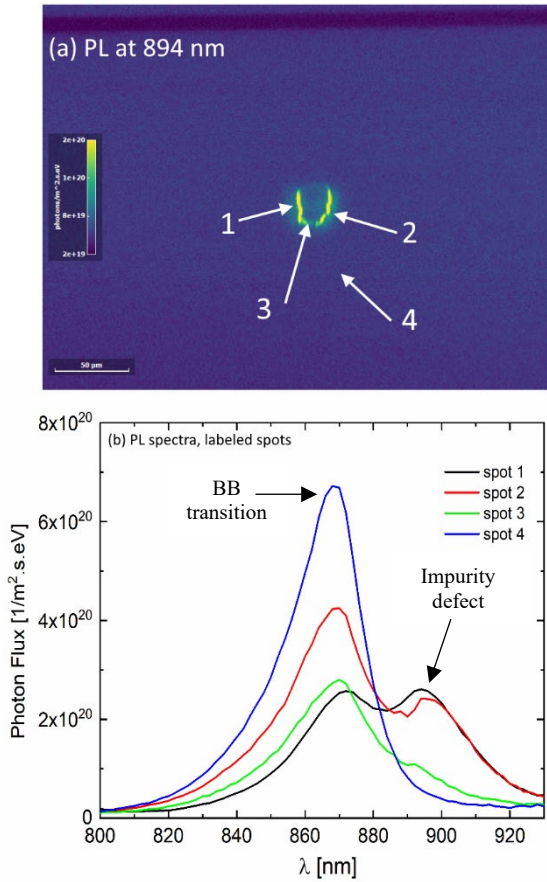
(a) PL at 894 nm

(b) PL spectra, labeled spots

BB transition

Impurity defect

- spot 1
- spot 2
- spot 3
- spot 4

Fig. 3. (a) The PL image of a localized defect under the 20× objective at 894 nm and at 297 K, showing a strong radiative signal from a halo band of what is believed to be the site of Ga_{As} antisite defects. (b) Spectra from several labelled locations (tip of the arrow).

them, hence showing only the BB signal peaked at 870 nm at 297 K.

The PL curve below the band gap energy (>870 nm) sampled at the defect sites does not drop off to zero but rather displays a shallow tail distribution. In Fig. 3(a), we have magnified *defect 1* with a 20× objective for a better visualization. This image clearly reveals the previously-mentioned bright halo around the center of the defect at 894 nm. Spectrum sampling
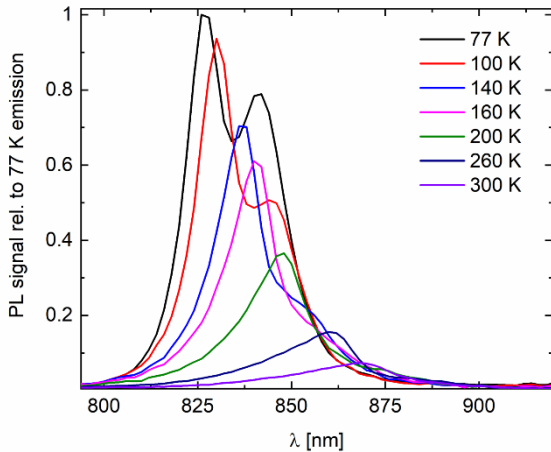

Fig. 4. Temperature dependence of a single defect spectra, showing the prominence of a sub-band gap defect peak at 77 K.

(Fig. 3(b)) of a few spots directly on and off the halo shows a double-peak distribution on the bright regions and reduced intensities at other areas. Therefore, the 870 nm peak is the BB transition, and the 894 nm peak indicates the formation of a defect sub-band gap transition at these particular locations.

Room temperature measurements alone are not sufficient to identify the nature of these sub-band gap defects and GaAs radiative peaks are usually studied at low temperatures, particularly at 77 K. We have performed preliminary temperature dependent measurements to better understand the evolution of the defect peak with temperature. These measurements, which have been performed with the 5× objective, are shown in Fig. 4 where we plot the normalized PL signal (relative to the 77 K PL) at one such defect site for several temperatures. Here, the PL signal is an average signal from the defect region and hence does not show a distinct double peak at 300 K. However, a double peak is clearly visible at 77 K, with the higher-wavelength peak emanating from the defect emission. From this plot, it is clear that the defect peak has a substantial temperature dependence and shows an activated behavior. The PL intensity of the BB peak usually increases substantially at lower T, as shown here, and the peak distribution becomes sharper due to the freezing of nonradiative recombination. The peak position also shifts to higher energy (1.50 eV, or 827 nm) due to the temperature dependence of the band gap energy [10].

Furthermore, we observe that the defect peak increases in intensity as T is lowered, at a rate faster than the BB peak, and reaches an almost comparable emission intensity as the BB peak at 77 K (dark curve). The defect peak position at 77 K is 1.473 eV (842 nm). This peak, particularly in Si-doped GaAs samples has been associated with gallium antisite defects (Ga_{As} or a Ga atom at an As site) or gallium vacancies that in large concentrations can act as a band of compensating acceptors causing the optical transition to shift from BB to band-to-impurity (i.e., electrons in the conduction band recombine with holes trapped on these acceptors) [11], [12]. This type of transition is often referred to as free-to-bound (FB) transition[13], [14]. Detailed temperature-dependent PL intensity measurements can reveal significant information regarding these defect transitions and will be discussed in a future work. Our preliminary results indicate an activation energy of about 41 meV for this transition. The peak position at 77 K can be slightly dependent on the Si dopant concentration with values reported between 1.45 eV and 1.47 eV from lightly doped to heavily doped materials. Since the defect peak in our samples is at 1.473 eV, we speculate a higher concentration of Si doping in the vicinity of these defects.

IV. CONCLUSIONS

Hyperspectral imaging in PL mode has been successfully used to study local radiative defects in GaAs solar cells. In addition to pinhole defect sites, a halo-like, radiative transition with peak emission at 894 nm at room T has been observed at several sites including around the pinhole defects. Low temperature imaging indicates that these defects are likely composed of Ga antisite point defects, energetically located about 41 meV above the valance band edge.

REFERENCES

[1] A. Delamarre, L. Lombez, and J. F. Guillemoles, "Characterization of solar cells using electroluminescence and photoluminescence hyperspectral images," in *Proc. of SPIE*, Feb. 2012, vol. 8256, p. 825614, doi: 10.1117/12.906859.

[2] E. Gaufrès *et al.*, "Hyperspectral Raman imaging using Bragg tunable filters of graphene and other low-dimensional materials," *J. Raman Spectrosc.*, vol. 49, no. 1, pp. 174–182, Jan. 2018, doi: 10.1002/jrs.5298.

[3] I. Burud, T. Mehl, A. Flo, D. Lausch, and E. Olsen, "Hyperspectral photoluminescence imaging of defects in solar cells," *J. Spectr. Imaging*, vol. 5, no. August, pp. 1–5, 2016, doi: 10.1255/jsi.2016.a8.

[4] Q. Chen *et al.*, "Impact of Individual Structural Defects in GaAs Solar Cells: A Correlative and In Operando Investigation of Signatures, Structures, and Effects," *Adv. Opt. Mater.*, vol. 9, no. 2, p. 2001487, Jan. 2021, doi: 10.1002/adom.202001487.

[5] S. M. Chavali, J. Roller, M. Dagenais, and B. H. Hamadani, "A comparative study of subcell optoelectronic properties and energy losses in multijunction solar cells," *Sol. Energy Mater. Sol. Cells*, vol. 236, no. August 2021, p. 111543, Mar. 2022, doi: 10.1016/j.solmat.2021.111543.

[6] B. H. Hamadani, "Understanding photovoltaic energy losses under indoor lighting conditions," *Appl. Phys. Lett.*, vol. 117, no. 4, p. 043904, Jul. 2020, doi: 10.1063/5.0017890.

[7] NIST Disclaimer: "Certain commercial equipment, instruments, software, or materials are identified in this paper to specify the experimental procedure adequately. Such identification is not intended to imply recommendation or endorsement by the National Institute of Standards and Technology, nor is it intended to imply that the materials or equipment identified are necessarily the best available for the purpose".

[8] M. A. Stevens *et al.*, "High Growth Rate Rear-Junction GaAs Solar Cell with a Distributed Bragg Reflector," in *2021 IEEE 48th Photovoltaic Specialists Conference (PVSC)*, Jun. 2021, pp. 0342–0345, doi: 10.1109/PVSC43889.2021.9518409.

[9] K. J. Schmieder *et al.*, "Effect of Growth Temperature on GaAs Solar Cells at High MOCVD Growth Rates," *IEEE J. Photovoltaics*, vol. 7, no. 1, pp. 340–346, Jan. 2017, doi: 10.1109/JPHOTOV.2016.2614346.

[10] I. Vurgaftman, M. P. Lumb, and J. R. Meyer, *Bands and Photons in III-V Semiconductor Quantum Structures*. Oxford University Press, 2020.

[11] L. Pavesi, M. Henini, and D. Johnston, "Influence of the As overpressure during the molecular beam epitaxy growth of Si-doped (211)A and (311)A GaAs," *Appl. Phys. Lett.*, vol. 2846, no. November 1994, p. 2846, 1995, doi: 10.1063/1.113449.

[12] N. H. Ky and F. K. Reinhart, "Amphoteric native defect reactions in Si-doped GaAs," *J. Appl. Phys.*, vol. 83, no. 2, pp. 718–724, Jan. 1998, doi: 10.1063/1.366743.

[13] T. Unold and L. Gütay, "Photoluminescence Analysis of Thin-Film Solar Cells," in *Advanced Characterization Techniques for Thin Film Solar Cells*, vol. 1–2, Weinheim, Germany: Wiley-VCH Verlag GmbH & Co. KGaA, 2016, pp. 275–297.

[14] S. Levcenko, V. E. Tezlevan, E. Arushanov, S. Schorr, and T. Unold, "Free-to-bound recombination in near stoichiometric Cu2ZnSnS4 single crystals," *Phys. Rev. B*, vol. 86, no. 4, p. 045206, Jul. 2012, doi: 10.1103/PhysRevB.86.045206.